Biochimica et Biophysica Acta 1837 (2014) 1284–1292

Contents lists available at ScienceDirect

Biochimica et Biophysica Acta

journal homepage: www.elsevier.com/locate/bbabio

Functional and molecular characterization of plastid terminal oxidase from rice (*Oryza sativa*)

Qiuju Yu [a], Kathleen Feilke [b], Anja Krieger-Liszkay [b], Peter Beyer [a,*]

[a] Faculty of Biology, University of Freiburg, D-79104 Freiburg, Germany
[b] Commissariat à l'Energie Atomique (CEA) Saclay, iBiTec-S, CNRS UMR 8221, Service de Bioénergétique, Biologie Structurale et Mécanisme, 91191 Gif-sur-Yvette Cedex, France

ARTICLE INFO

Article history:
Received 12 February 2014
Received in revised form 9 April 2014
Accepted 12 April 2014
Available online 26 April 2014

Keywords:
Plastid terminal oxidase
PTOX
Reactive oxygen species
Photosynthesis
Carotene desaturation
Plastoquinone

ABSTRACT

The plastid terminal oxidase (PTOX) is a plastohydroquinone:oxygen oxidoreductase that shares structural similarities with alternative oxidases (AOX). Multiple roles have been attributed to PTOX, such as involvement in carotene desaturation, a safety valve function, participation in the processes of chlororespiration and setting the redox poise for cyclic electron transport. We have investigated a homogenously pure MBP fusion of PTOX. The protein forms a homo-tetrameric complex containing 2 Fe per monomer and is very specific for the plastoquinone head-group. The reaction kinetics were investigated in a soluble monophasic system using chemically reduced decyl-plastoquinone (DPQ) as the model substrate and, in addition, in a biphasic (liposomal) system in which DPQ was reduced with DT-diaphorase. While PTOX did not detectably produce reactive oxygen species in the monophasic system, their formation was observed by room temperature EPR in the biphasic system in a [$DPQH_2$] and pH-dependent manner. This is probably the result of the higher concentration of DPQ achieved within the partial volume of the lipid bilayer and a higher Km observed with PTOX-membrane associates which is ≈47 mM compared to the monophasic system where a Km of ≈74 μM was determined. With liposomes and at the basic stromal pH of photosynthetically active chloroplasts, PTOX was antioxidant at low [$DPQH_2$] gaining prooxidant properties with increasing quinol concentrations. It is concluded that in vivo, PTOX can act as a safety valve when the steady state [PQH_2] is low while a certain amount of ROS is formed at high light intensities.

1. Introduction

The plastid terminal oxidase gene, initially identified through transposon tagging [1] and shown to map to the *immutans (im)* locus of *Arabidopsis thaliana* [2], codes for a plastid quinol:oxygen oxidoreductase, termed plastid terminal oxidase (PTOX). This catalytic function is indicated by (limited) sequence similarity to mitochondrial alternative oxidase (AOX). However, functional residues such as the four glutamates and two histidines, for instance, thought to coordinate two Fe ions, are highly conserved [3]. Their function in providing the structural basis for the active diiron carboxylate center has recently been confirmed by the structural elucidation of AOX from *Trypanosoma brucei* [4]. In addition, hydroquinone oxidation by PTOX was also shown in vivo [5] and in vitro [6].

The lack of PTOX caused by the *im* mutation leads to a variegated leaf phenotype i.e. with sectors showing either a bleached or wild-type appearance. White sectors accumulate phytoene; they are defective in phytoene desaturation catalyzed by phytoene desaturase (PDS) and these areas are therefore amenable to photobleaching [7]. This corroborates older data showing that PDS—directly or indirectly—requires quinones for activity ([8,9]. The white/green sectors are thought to arise during a crucial early phase in chloroplast development during which an optimal carotenoid complement is critically important. Only those cells with plastids successfully escaping this phase by eventually developing chloroplasts develop green sectors documenting that PTOX is then largely dispensable in carotene desaturation, the redox regulation of the plastoquinone pool being dominated by photosynthetic electron transport. PDS, requiring the midpoint potential of the PQ/PQH_2 redox pair for optimal function [10] is thus largely PTOX-independent in mature chloroplasts; conversely it is fully PTOX-dependent in non green plastids. Accordingly, tomato fruit defective in PTOX (*ghost*) have white fruit under high light conditions while mature leaves are hardly affected [11].

Abbreviations: DPQ, decyl-plastoquione; PTOX, plastid terminal oxidase; nOG, n-octyl β-D-glucopyranoside; DCPIP, 2,6-dichlorophenol-indophenol-Na; IPTG, isopropyl β-D-1-thiogalactopyranoside; BSA, bovine serum albumin; DoDm, n-dodecyl β-D-maltoside; DeDm, n-decyl β-D-maltoside; CHAPS, 3-[(3-cholamidopropyl)dimethylammonio]-1-propanesulfonate; LDAO, *N,N*-dimethyldodecylamine *N*-oxide; CMC, critical micelle concentration; GPC, gel permeation chromatography; SOD, superoxide dismutase

* Corresponding author at: University of Freiburg, Faculty of Biology, Schänzlestr. 1, 79104 Freiburg, Germany. Tel.: +49 761 203 2529; fax: +49 761 203 2675.
E-mail address: peter.beyer@biologie.uni-freiburg.de (P. Beyer).

http://dx.doi.org/10.1016/j.bbabio.2014.04.007
0005-2728/

What is the role of PTOX in chloroplasts, given that it is dispensable for carotenogenesis? The "safety valve" function, which is a protective function against over-reduced states under high light and other stress conditions has frequently been put forward. For instance, the alpine plant *Ranunculus glacialis* under light stress at increasing altitudes [12], the halophyte *Thellungiella halophila* under salt stress [13] and *Brassica fruticulosa* under temperature and light stress [14], all respond by increasing PTOX levels. The current interpretation is that PTOX acts as an alternative electron sink consuming excess photosynthetically generated electrons avoiding over-reduction of the quinone pool. Reduction of oxygen to water has been assumed thus preventing the formation of toxic ROS. However, this is not undisputed. PTOX has been reported to not protect from photoinhibition in overexpressing Arabidopsis plants [15]. Moreover, PTOX-overexpressing plants are not protected in high light; rather the opposite is true as witnessed by strongly increased superoxide and hydroxyl radical levels [16]. Similarly, overexpression of PTOX from *Chlamydomonas reinhardtti* achieved by chloroplast transformation of tobacco led to plants which were more sensitive to light than the wild type [17]. Moreover, PTOX activity measured non-invasively was shown under diverse conditions to be about two orders of magnitude lower than that of its competitor for hydroquinones, the linear electron transport, which is not compatible with a safety valve function [18].

Additional functions attributed to PTOX relate to its participation in the chlororespiratory pathway. Here, the reduction of the PQ pool by ferredoxin:quinone reductase (FQR), or non-photochemically by NADPH through the plastid-encoded NDH complex or an NADPH:plastoquinone oxidoreductase requires a terminal oxidase that is thought to be PTOX [19,5]. Moreover, based on functional measurements, PTOX is also thought to regulate the cyclic electron circuits around PSI by fine-tuning the redox state of electron carriers [20,18].

Thus, several vitally important PTOX functions have been indicated by the use of reverse genetics and by spectroscopic measurements: carotene desaturation, a safety valve function, involvement in chlororespiration and in cyclic electron transport around PSI. However, the necessary interpretations all suffer from the fact that there is hardly any knowledge on the intrinsic properties of PTOX. Investigations "close to the enzyme" have been presented by Josse et al. [6] using *Escherichia coli* expressed protein, however these experiments suffer from the fact that complex *E. coli* membrane preparations were used to which the protein is bound i.e. that PTOX was investigated in the presence of the respiratory redox chain resulting in a complex mix of a multitude of redox mediators.

We therefore set out to fill this research gap by investigating PTOX from *Oryza sativa* only using a minimum of components such as purified recombinant protein, hydroquinones in free form or embedded into liposomal membranes. The results obtained shed light on the oligomeric assembly of PTOX, its kinetic properties and identify conditions under which ROS can be produced.

2. Material and methods

2.1. Chemicals used

Phusion™ High-Fidelity DNA Polymerase was a product of Finnzymes. Amylose resin and restriction enzymes were from New England BioLabs (UK). n-Octyl β-D-glucopyranoside was purchased from AppliChem (Germany). Phenyl-p-benzoquinone, dimethoxy-5-methyl-1,4-benzoquinone, 2,5-dimethyl-benzoquinone, 2,6-dimethyl-benzoquinone, 3,5-di-tert-butyl-1,2-benzoquinone, 2,5-dichloro-benzoquinone, and 2,6-dichloro-benzoquinone were from Sigma, Fluka and Kodak. 2,3-dimethyl-benzoquinone was from SynChem OHG (Germany). Gel Filtration LMW and HMW Calibration Kits were purchased from GE Healthcare. The following quinones and other fine chemicals were purchased from Sigma-Aldrich: duroquinone (2,3,5,6-tetramethyl-1,4-benzoquinone), decyl-plastoquinone (2,3-methyl-5-decyl-1,4-benzoquinone), octyl-gallate (3,4,5-trihydroxybenzoic acid-n-octylester), DCPIP (2,6-dichlorphenol-indophenol-Na), p-benzoquinone, decyl-ubiquinone (2,3-dimethoxy-5-methyl-6-decyl-1,4-benzoquinone), and vitamin K1 (2-methyl-3-phytyl-1,4-naphthoquinone).

2.2. Cloning and DNA constructs

To clone OsPTOX (Acc. AF085174.3) lacking a predicted 35-amino-acid transit peptide (ChloroP 1.1 software) the corresponding cDNA was synthesized by GenScript (Germany). Primers OsPTOX Fw1 5′-AGTCAT ATGGGTACCGTCGGCACCGTCGCC-3′ (*Kpn*I) and OsPTOX + Stop Rs1 5′-GCAAGCTTGGATCCTCACTCTTTACTCACAAGAG-3′ (*Bam*HI) were used for introducing restriction sites by PCR amplification using Phusion™ High-Fidelity DNA Polymerase. The purified PCR product was inserted into pBAD-TOPO vector (Invitrogen) by TA cloning and the resulting vector pBAD-OsPTOX + TGA verified by sequencing. The *Kpn*I/*Bam*HI fragment was inserted in-frame into a series of Gateway derived destination vectors as described [21,22]. The expression plasmids pHGW-OsPTOX, pHMGW-OsPTOX, pHGGW-OsPTOX, pHNGW-OsPTOX and pHXGW-OsPTOX encode the corresponding fusion proteins His6-OsPTOX; His6-MBP-OsPTOX (MBP: maltose-binding protein); His6-GST-OsPTOX (GST: glutathione S-transferase); His6-NusA-OsPTOX (NusA:N-utilizing substance A) and His6-TRX-OsPTOX (TRX: thioredoxin). The Gateway empty vector pHMGW which encodes only His6-MBP was used as control.

2.3. MBP-OsPTOX expression and purification

All plasmids were transformed into BL21(DE3) *E. coli* cells. 2 ml of overnight cultures of transformed cells was inoculated into 400 ml of 2*YT-medium, grown at 37 °C to an OD_{600} of 0.8 and induced with IPTG (0.2 mM). After induction overnight at 16 °C the cells were harvested and either used directly or frozen at −80 °C.

Purification was carried out on ice. Cells were resuspended in buffer A (25 mM sodium-phosphate buffer pH 7.6, $MgCl_2$ 2.5 mM, NaCl 300 mM, glycerol 15 vol.%) and disintegrated by three passages through a French Pressure Cell at 18,000 psi. After centrifugation at 28,000 *g* for 40 min the supernatant was solubilized for 30 min on ice by slowly adding 5 X CMC n-octyl β-D-glucopyranoside (nOG; 1 X CMC = 25 mM) and then applied to Amylose resin (BioLab). After washing thoroughly with buffer A containing 1 X CMC nOG; the elution was accomplished with buffer B (50 mM Tris–HCl pH 8.0, $MgCl_2$ 2.5 mM, glycerol, 10 vol.%) containing 1 X CMC nOG and 10 mM maltose.

Further purification of His6-MBP-PTOX was achieved by ion exchange chromatography using an ÄKTA-explorer FPLC (GE Healthcare) with MONO Q 5/50 GL column (GE Healthcare) equilibrated with buffer B containing 1 X CMC nOG and 180 mM NaCl. 500 μl of Amylose-purified PTOX was loaded with the same buffer and the column developed with a linear gradient using buffer B in the presence of 1 X CMC nOG and 500 mM NaCl. This was followed by a washing step with the same buffer containing 1 M NaCl.

The peak eluting at about 220 mM NaCl was collected and the purity was checked by SDS-PAGE using 10% polyacrylamide gels. Further purification and MW determination were achieved by gel permeation chromatography (GPC) using a Superdex 200 10/300 GL column (GE Healthcare) equilibrated with buffer B containing 1 X CMC nOG and calibrated with the LMW and HMW Calibration Kit (GE Healthcare). Proteins resolved by SDS-PAGE were detected using Coomassie Brilliant Blue G250 (Sigma-Aldrich). Protein quantification was done using the Bradford reagent.

2.4. Enzyme assays and measurements

Protein-free liposomes containing the quinone acceptors were prepared with 10 mg/ml of soybean lecithin (Sigma-Aldrich) in buffer B, as described [23–25]. The quinone/lipid ratio was estimated with the

average molecular mass of 766 Da for lecithin. DPQ that was not incorporated into liposomal membranes was washed away with n-pentane according to [26]. To quantify effectively incorporated DPQ an aliquot of the pentane-washed liposome suspension was extracted twice with 1 vol. of chloroform/methanol 2:1 (*v*/*v*). The combined organic phases were dried and redissolved in 50 μl chloroform of which 15 μl was analyzed using an UFLC Prominence system (Shimadzu) employing a 3 μm C30 reversed phase column (YMC-Europe) with the solvent system A (MeOH/tert-butylmethyl ether (TBME)/water 5:1:1, *v*/*v*/*v*) and B (MeOH/TBME 1:3, *v*/*v*). The linear gradient was developed from 60% A to 0% A within 13 min at a flow rate of 0.6 ml/min. An isocratic segment, run for 5 min at 0% A completed the separation program. DPQ peaks were integrated electronically at their λ_{max} (257 nm) with the aid of the "maxplot" function of the software. Calibration curves made with standard solutions allowed calculating DPQ concentrations.

When not indicated differently, assays with liposome-bound DPQ coupled with human DT diaphorase contained 50 μl of liposome (500 μg lipid) harboring different concentrations of DPQ, 10 μg of MBP-OsPTOX, 10 μg of DT diaphorase (Sigma-Aldrich) and 200 μM NADH. Buffer B was added to 698 μl, then 10 μg of OsPTOX (2 μl) was added to start the reaction. Potentiometric measurements were carried out with an Oxygraph plus (Hansatech, Germany) oxygen electrode at 35 °C. At this temperature, both OsPTOX and human DT diaphorase are at their temperature optimum (comp. Supplementary Fig. 2B). To conduct assays containing free $DPQH_2$, the concentration of DPQ in methanol stock solution was determined spectro-photometrically (Shimadzu, UV-2501PC) using ε_{257} nm = 17.94 l $mmol^{-1}$ cm^{-1} [27] and adjusted to 10 mM. Reduction was carried out with an excess of solid $NaBH_4$. After 15 min incubation on ice the reductant was decomposed with a few microliters of 3 M HCl. Aliquots were directly applied to the assays.

The pH dependence of OsPTOX activity was determined using 50 mM Tris–HCl and 25 mM Na-phosphate buffer both containing 2.5 mM $MgCl_2$, 10 vol.% glycerol and 1 X CMC nOG for pH 5.8–8.0 and pH 7.0–9.0, respectively.

The formation of superoxide and H_2O_2 was investigated by adding catalase (CAT, 600U) and superoxide dismutase (SOD, 20U) during the measurement to observe kinetic changes. We also routinely added the enzymes at the end of the reaction to examine the potential formation of dioxygen. In addition, trace amount production of H_2O_2 was assayed with "Amplex® Red hydrogen peroxide assay kit" (Invitrogen) or by the fluorescent method with the europium–tetracycline 3:1 complex (Eu3Tc; Sigma-Aldrich) according to [28].

2.5. Room-temperature EPR

Spin-trapping assays with 4-pyridyl-1-oxide-*N*-*tert*-butylnitrone (4-POBN) (Sigma-Aldrich) were carried out to detect the formation of hydroxyl radicals. (The spin trapping assay contained 50 mM 4-POBN, 4% ethanol, 50 μM Fe-EDTA. EPR spectra were recorded at room temperature in a standard quartz flat cell using an ESP-300 X-band spectrometer (Bruker, Germany). The following parameters were used: microwave frequency 9.73 GHz, modulation frequency 100 kHz, modulation amplitude 1 G, microwave power 6.3 mW, receiver gain 2×10^4, time constant 40.96 ms, and number of scans 4.

2.6. Native gel electrophoresis

Non-denaturing gel electrophoresis (omitting SDS in all buffers) was used to determine the oligomeric assembly of OsPTOX. Purified protein was applied to 7.5% native polyacrylamide gels. Electrophoresis was carried out using 25 mM Tris/200 mM glycine buffer. Bovine serum albumin (BSA), known to form homo-oligomers, was used as a control.

2.7. Atomic absorption spectroscopy (AAS)

Purified OsPTOX tetramer was collected and the tetrameric assembly and quality of the preparation were checked by GPC on a Superdex 200 10/300 column and by SDS-PAGE. All buffers used were prepared with ultra-pure water (TraceSELECT H_2O, Sigma-Aldrich). Protein concentration was determined with the Bradford reagent using BSA (Sigma-Aldrich) as a standard. Fe content was measured at 248.3 nm with an Automated Graphite Furnace Atomic Absorption Spectrometer (Model AAS 5 EA, Carl Zeiss, Germany). A calibration curve within the required concentration range was established using a 25 μg/l Single-Element Iron AAS-standard-solution (Roth). Fe-contents in MBP-OsPTOX and in buffer controls were measured with two independent protein batches and at different MBP-OsPTOX dilutions (500–2000-fold). The pyrolysis temperature ramp used was from 500–1100 °C within 12 s. For each measurement, 3–4 readings were obtained and the average calculated.

3. Results and discussion

3.1. OsPTOX purification and oligomeric state

The cDNA of OsPTOX coding for the mature protein (with its transit sequence removed) was cloned into a series of Gateway-derived vectors to express five different N-terminal fusion proteins according to [21] in *E. coli* (BL21DE3). Among these variants His6-MBP-OsPTOX (hereafter MBP-OsPTOX) gave the best results producing a substantial proportion of the protein (~75%) in the membrane fraction, which was recovered at 140,000 ×*g* after the removing of inclusion bodies (about 25%) and cell debris at 13,000 ×*g*. This indicated that MBP-OsPTOX behaved as a membrane interacting protein in *E. coli*, as expected, despite the relatively large (43 kDa) N-terminal fusion. This fusion also gave the best protein yield upon purification and proved to be the most enzymatically active form as assessed potentiometrically by measuring the hydroquinone-dependent O_2 consumption rates (see below).

Taking advantage of the MBP-fusion, amylose resin was used for affinity purification, which gave better purity of MBP-OsPTOX as compared to the utilization of the His6-tag. Solubilization of the membrane-bound MBP-OsPTOX from *E. coli* membranes was optimized using the detergents Tween 20, nOG, DoDm, CHAPS, DeDm, LDAO and Triton X 100. nOG turned out to be best-suited in decreasing notorious protein aggregation and in removing contaminations while maintaining the enzymatic activity. SDS-PAGE analysis showed the expected molecular mass of the purified fusion protein of 76.8 kDa (Fig. 1A).

Subsequent gel permeation chromatography (GPC) indicated purified MBP-OsPTOX to form a defined homo-oligomeric complex. A typical GPC run is shown in Fig. 1B, where MBP-OsPTOX eluted as a solitary peak occasionally followed by a minor contaminant, which was mass spectrometrically identified as MBP. Higher aggregated forms eluting in the void volume were not present under the conditions used but formed massively in the presence of detergents other than nOG. Homo-tetrameric association (a molecular mass of >300 kDa) of MBP-OsPTOX was indicated using a calibrated Superdex 200 10/300 column (Supplemental Fig. 1) and confirmed on native polyacrylamide gels using BSA, known to form distinct homo-oligomers, as a marker [29] (Fig. 1C). This showed that MBP-OsPTOX existed mainly as tetramer that dissociated to a certain extent during electrophoresis into the trimeric, dimeric and monomeric forms. The tetramer peak collected from GPC showed to contain MBP-OsPTOX in an essentially homogeneous form (Fig. 1A, lane 3). The preparation was enzymatically active and showed to maintain the activity at −80 °C for several months. Efforts to dissociate the MBP-OsPTOX tetramer by varying various compositional buffer parameters (pH, ion strength, reducing agents) were not successful, all leading to aggregated enzymatically inactive forms.

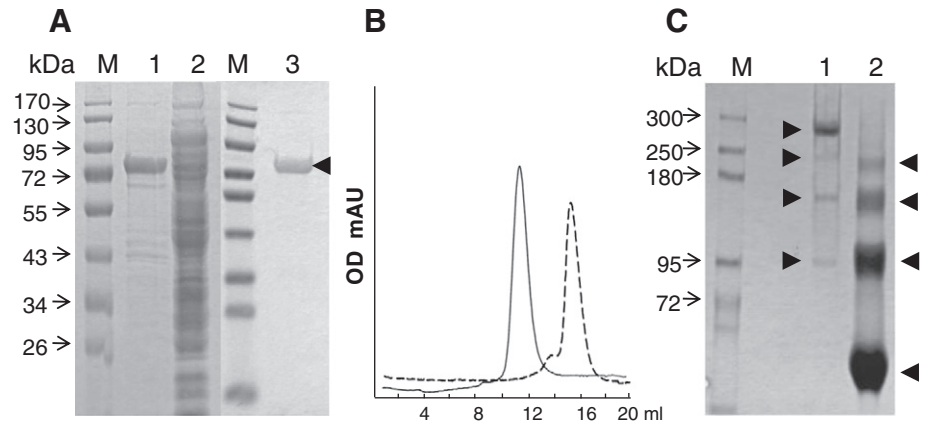

Fig. 1. Purification of MBP-OsPTOX. A, SDS-PAGE. Lane 1, fraction after affinity purification; lane 2, cell lysate after induction; lane 3, tetramer fraction after GPC; M, size marker proteins. The arrowhead denotes the position of MBP-OsPTOX with its expected electrophoretic mobility representing 76.8 kDa. B, GPC purification of the affinity-purified MBP-OsPTOX (solid line) and MBP (dashed line) on a Superdex 200 FPLC column. The elution volume of MBP-OsPTOX indicated homo-oligomeric assembly (see lane 3 in Fig. A). C, Native PAGE analysis of GPC-purified MBP-OsPTOX (lane 1) and of BSA (lane 2). Arrowheads denote, in descending order, tetra-, tri-, di- and monomeric assemblies for both proteins.

Although MBP is known to exist as a monomer [30] and has no reputation of fostering the oligomeric association of fusion proteins, we expressed His6-MBP in BL21(DE3) *E. coli* cells, and subjected the expressed protein to the same purification protocol as used with MBP-OsPTOX. Upon GPC, His6-MBP migrated in its monomeric form, as expected (Fig. 1B), thus indicating that the tetrameric assembly of MBP-OsPTOX was formed through interactions of the PTOX proportion of the fusion protein.

Tetrameric assembly is surprising considering the fact that AOX from *Trypanosoma bruzei* crystallized in the form of a homodimer [4]. In addition, the number of available Fe redox centers in a functional tetramer seemingly exceeds the amount needed to reduce oxygen to water, in the light of a diiron center per monomer. This diiron configuration appears conceivable based on our measurements (see below) and the conservation of Fe-coordinating glutamates and histidines among AOX and PTOX.

Crystallization attempts were not successful. MBP fusions are known to be notoriously difficult in this respect caused by the conformational heterogeneity induced by the fusion tag (for review, see [31]). However, MBP cleavage (using a 3C protease site introduced for this purpose) resulted in the precipitation of this membrane protein and the recommended mutagenesis of sites within the linker and the MBP portion to reduce surface entropy using plasmids described in [32] and kindly provided by the authors of this publication did not result in sufficient improvement at this occasion.

3.2. Enzymatic activity in the absence of liposomal membranes

For routine enzymatic analysis, we scaled up the protein preparation by replacing the second (GPC) purification step by ion exchange chromatography using a MONO Q 5/50 GL column. This produced very good yields of the active tetramer, as estimated by GPC (Supplemental Fig. 1B). $NaBH_4$-reduced decyl-plastoquinone added from a methanol stock solution was used as substrate in assays that did not contain liposomes. Enzymatic activity was assessed by measuring O_2 reduction with an oxygen electrode. Standard assay conditions were established based on kinetic optimizations at a 100 μM decyl-plastohydroquinone concentration. Purified MBP-OsPTOX tetramer showed a linear correlation of activity with protein concentration up to 15 μg per 700 μl assay volume (Supplemental Fig. 2A) and a temperature optimum from ca. 35 °C to 42 °C (Supplemental Fig. 2B). A protein concentration of 10 μg/700 μl was therefore selected yielding a linear reaction for 3 min (compare Fig. 6) with a conversion rate of 12.2 ± 1.2 μmol O_2 min^{-1} mg^{-1} at 35 °C.

Under these conditions, the pH dependence of the reaction was examined. As shown in Fig. 2, MBP-OsPTOX maintained activity in a range from pH 5.8–8.5 with a shallow optimum at about pH 7.5. Further pH increase led to decreased activity. This is inconsistent with previous observations with *E. coli* membrane preparations [6], where optimal activity was observed at the alkaline edge. This may be attributed to the fact that membrane preparations were used and NADH as the electron donor. It appears conceivable that ubiquinone reduction through NADH:ubiquinone oxidoreductases in the presence of many additional redox active components such as the three *E. coli* quinol oxidases, for instance, may (in the presence of cyanide) result in alterations of the membrane redox homeostasis in response to variations of the ambient pH. PTOX is dependent on these alterations possibly affecting the redox state of the plastoquinone pool—this might have partially masked the pH dependence of PTOX.

Quinol electron donor specificity was investigated using a series of quinone head-groups differing in ring types (benzo- and naphthoquinones) and substituents (see Supplemental Fig. 3 for structures). Two of these, namely the head group of ubiquinone (2, 3-dimethoxy-5-methyl-1,4-benzoquinone) and of plastoquinone (2,3-dimethyl-p-benzoquinone) were also used in their C_{10} alkylated forms, i.e. decyl-ubiquinol and decyl-plastoquinol ($DPQH_2$, with the

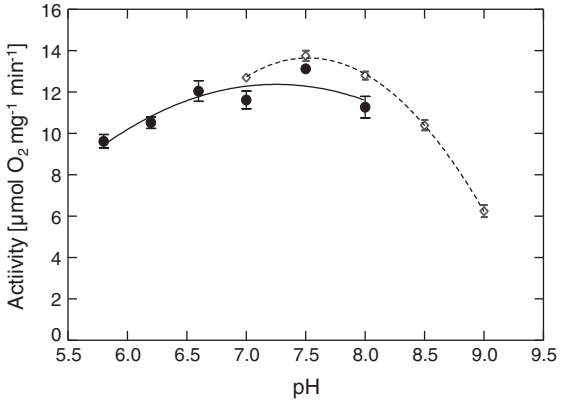

Fig. 2. pH dependence of the MBP-OsPTOX reaction. Standard assay conditions using 100 μM decyl-plastohydroquinone were used. The assays were made in the presence of 10 μg protein per 700 μl assay volume. Activities were determined from electronically recorded potentiometric plots using the Oxygraph Plus software of the Oxygen electrode used. The buffers used were 50 mM Tris–HCl (filled symbols) and 25 mM Na-phosphate buffer (open symbols) both containing 2.5 mM $MgCl_2$, 10 vol.% glycerol and 1 X CMC nOG.

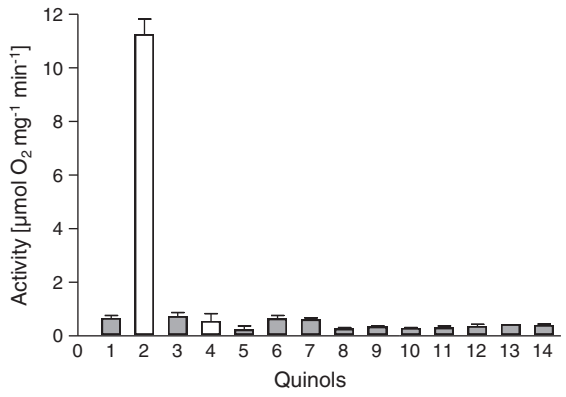

Fig. 3. Effectiveness of different hydroquinones as MBP-OsPTOX electron donors. White bars, decyl-hydroquinones; the corresponding head-groups are on the right side of the white bars. The hydroquinones used were prepared freshly by reduction with $NaBH_4$. (1) 2,3,5,6-tetramethyl-p-benzoquinone (duroquinone), (2) decyl-plastoquinone, (3) 2,3-dimethyl-p-benzoquione, (4) decyl-ubiquinone, (5) 2,3-dimethoxy-5-methyl-p-benzoquinone, (6) 2,5-dimethyl-p-benzoquinone, (7) 2,6-dichlorphenol-indophenol-Na (DCPIP) (8) 3,5-di-tert-butyl-1,2-p-benzoquinone, (9) p-benzoquinone, (10) 2,5-dichloro-p-benzoquinone, (11) 2,6-dichloro-p-benzoquinone, (12) phenyl-p-benzoquinone, (13), 2,6-dimethyl-p-benzoquinone, and (14) phylloquinone (2-methyl-3-phytyl-1,4-naphtoquinone). All hydroquinones were used at a 100 µM concentration.

decyl groups attached to the C_5 ring atom, mimicking prenylation). As shown in Fig. 3, pronounced specificity for $DPQH_2$ (2) was observed; all other hydroquinones used were much less effective. In contrast to $DPQH_2$, its head group, 2,3-dimethyl-p-benzoquinol (3), was ineffective as well. A second equivalent pair, namely decyl-ubiquinol (4) and its head group (5); 2,3-dimethoxy-5-methyl-p-benzoquinol) were both ineffective. These observations are in agreement with the suggestion that specificity resides in both, the quinol head-group and a component contributed by the hydrophobic tail.

Kinetic analyses were carried out with freely diffusible $DPQH_2$ at optimized conditions revealing a Vmax of 16.6 ± 0.8 µmol O_2 mg^{-1} min^{-1} and a Km of 74 ± 10 µM (Fig. 4A).

3.3. Enzymatic activity with liposomal-bound $DPQH_2$

PTOX must interact with thylakoid membranes, to access plastohydroquinone. If essential characteristics are maintained in MBP-OsPTOX, the fusion protein should be capable in utilizing this electron donor when membrane-bound. Therefore, DPQ was incorporated into protein-free liposomes. Because of known problems encountered when partitioning quinones quantitatively into artificial membranes, we used n-pentane washing of liposomes which removes all the quinone present in water but does not deplete quinone that is incorporated in membranes [26]. The partition of DPQ (instead of the reduced form) was assessed since quinols suffer from reoxidation during pentane washing. HPLC analysis revealed that packing efficiency was linear over the concentration range of free DPQ used (0–2.5 mM) resulting in ca. 40% incorporation.

For kinetic analyses in a biphasic system the DPQ concentrations must refer to the actual concentration within the "two dimensional" plane of the lipid bilayer. This depends on the molecular volume of the lipid within lipid bilayers immersed in water. This has been calculated and experimentally confirmed [33]. Using the average molecular volume of the PC molecule of 1205 $Å^3$, the molarity (1.05 mM) of PC present in the assay and N_A, the volume of the lipid phase in the 700 µl aqueous assay volume can be calculated (0.53 µl). Knowing the partition behavior of DPQ the actual molar concentration of DPQ within the lipid phase of the pentane-washed liposomes can be calculated and this was also analytically confirmed by quantitative HPLC.

To reduce the lipid-incorporated DPQ, we then used DT-diaphorase (NAD(P)H: quinone-acceptor oxidoreductase) in the presence of 800 µM NADH [34]. Initial reaction velocities were measured

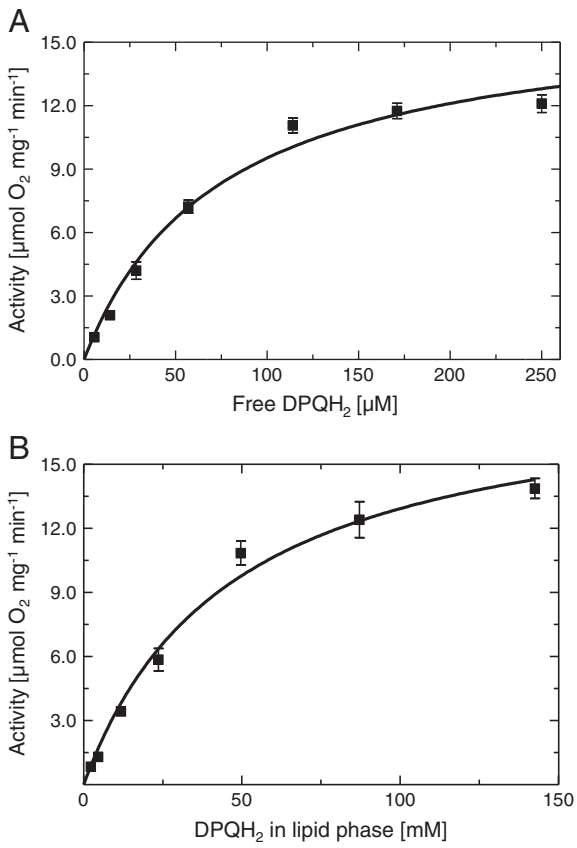

Fig. 4. Kinetic dependence of the reaction on free vs. membrane-bound decyl-plastoquinone. (A) Oxygen consumption at varying free $DPQH_2$ concentrations (in the absence of liposomes). Assays were conducted in standard reactions (buffer B pH 8; 10 µg MBP-OsPTOX in 700 µl). Freshly $NaBH_4$-reduced DPQ was used as the reductant. (B) Oxygen consumption at varying membrane-bound DPQ concentrations. DPQ was reduced at the expense of NADH (200 µM) through the action of standard DT diaphorase coupled assays. The curves in (A) and (B) were fitted with the Graphpad Prism 5.02 software using the Michaelis–Menten equation; $R^2 = 0.98$. Symbols represent the mean of at least three replicate experiments (±SE).

potentiometrically. As shown in Fig. 4B this resulted in a Km for $DPQH_2$ of 47 ± 0.6 mM and a Vmax of 19.01 ± 1.1 µmol O_2 mg^{-1} min^{-1}. Compared to the data obtained in the absence of liposomes with freely diffusible electron donor (Fig. 4A), the enzyme system exhibited a comparable value for Vmax, but the Km was much higher. This indicates that the reaction proceeded kinetically similar as with freely diffusible $DPQH_2$. However, liposomes (in which the local decyl-PQ concentrations are comparatively very high) introduce an unknown constraint negatively affecting substrate accessibility to the enzyme´s active center. Moreover, the kinetics of the DT-diaphorase reaction and the diffusion of the hydroquinone within the lipid phase might add to the phenomenon. Finally, it cannot be excluded that there is a contribution of the MBP fusion that might hinder the topologically correct membrane association of the protein.

3.4. Iron content of MBP-OsPTOX

Concentrated purified MBP-OsPTOX showed a pale greenish color indicating metal coordination. Iron requirement of MBP-OsPTOX was supported by the inhibitory effect of the metal chelator 1,10-phenanthroline that complexes Fe(II) [35]. The inhibitor–activity relation was biphasic (Fig. 5) with a strong inhibition to about 67% in the 1–5 µM range ($K_{HIGH} = 0.32$ $µM^{-1}$) while the second phase was much less responding ($K_{LOW} = 0.0015$ $µM^{-1}$) thus with a ratio of 209. This is indicative of two populations of Fe(II) differing in their accessibility towards the chelator.

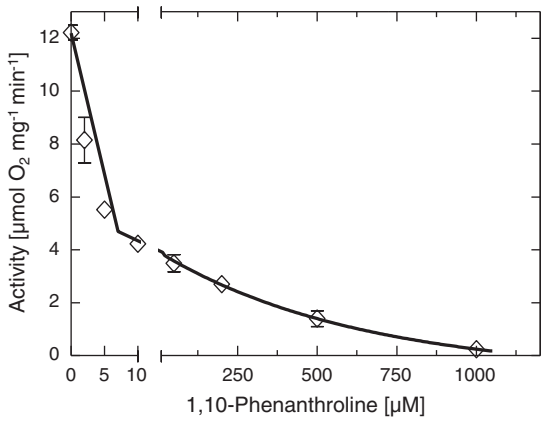

Fig. 5. Inhibitory effect of 1,10-phenanthroline on MBP-OsPTOX activity. MBP-OsPTOX (10 µg/700 µl) was pretreated for 10 min with increasing amounts of 1,10-phenanthroline in the presence of liposomes containing DPQ (100 µM) and NADH (200 µM). The reaction was started by adding DT-diaphorase (10 µg/700 µl) and the reaction velocities determined potentiometrically. The curve was fitted with the GraphPad Prism 5.02 software using the two phase exponential decay model. Symbols represent the mean of three replicates (±SE).

The iron content was measured by Atomic Absorption Spectroscopy using MBP-OsPTOX preparations that were made using buffers prepared with ultra-pure water. The MBP-OsPTOX tetramer fraction was stringently collected and protein concentrations determined. Control samples were collected from GPC runs without protein injection, serving as a blank. After subtraction and estimation based on a calibration curve, an average Fe/PTOX molar ratio of 2.25 ± 0.3 was determined with two independent batches of purified protein and 10 concentration-dependent technical replicates, each. Two irons per monomer are consistent with the motifs present in the primary structure and with the crystal structure obtained with the mitochondrial AOX [4].

3.5. Formation of water and/or ROS?

Mitochondrial AOX is generally thought to reduce oxygen to water and this is seemingly supported by electron balance: four irons present in the dimeric protein can catalyze the four step reduction of dioxygen at the expense of two hydroquinones. However, the evidence that supports this notion as reviewed in [36] has been questioned by Bhate and Ramasarma [37] suggesting the formation of H_2O_2. With respect to PTOX, the frequently quoted water formation is a mere assumption, lacking any experimental evidence, to our knowledge. We therefore set out to investigate product formation more closely, especially since the functional MBP-OsPTOX complex, a homo-tetramer accommodating 8 iron centers, possesses an excess of redox-active centers for the purpose.

To answer this question, we employed the coupled assay in which free DPQ (no liposomes) is reduced by DT-diaphorase at the expense of NADH. In addition, chemically reduced DPQ was used, all with the aim of stoichiometrically relating NADH-oxidation or $DPQH_2$-oxidation to oxygen reduction, measured potentiometrically in terms of O_2 consumption. At all NADH, $DPQH_2$- (both 2 electron carriers) and protein concentrations tested, the molar electron donor/O_2 ratio approximated very closely 2:1 (Table 1), with an average of all measurements of 2.08, which is in agreement with the four electron requirement for water formation. It is therefore concluded that water is by far the main product formed with freely diffusible soluble $DPQH_2$.

Parallels were conducted under most conditions in the presence of superoxide dismutase, catalase or both. Addition was done at the beginning of the measurement or at the end of the time course (Fig. 6). No changes in the rate or the generation of superoxide and hydrogen peroxide were observed. ROS potentially formed were also investigated by commercially available colorimetric methods (see Materials and methods); however, these all gave negative results. This further substantiates predominant water formation.

Phenanthroline inhibition (see above) might provide the means for introducing a dysbalance in the number of available redox-active iron centers. We therefore repeated the measurements at an intermediate 200 µM 1,10-phenantroline concentration (comp. Fig. 5). However, as seen in Fig. 6, the system remained robust towards such perturbation, since the time courses were not affected by SOD, by CAT and combinations of both. There was also no release of oxygen upon their addition after completion of the reaction. Similarly, the known PTOX inhibitor octyl-gallate which effectively inhibited the reaction (95% and 98% inhibition at 2 µM and 3 µM, respectively, see Supplementary Fig. 2C) did not provoke ROS formation when used at an intermediate concentration. The practically complete inhibition achieved (the residual 2% activity representing baseline drift; see Supplementary Fig. 2C) also indicates that the PTOX preparation used in our experiments is not contaminated by the three heme-containing alternative terminal quinol oxidases of

Table 1
Reductant/O_2 consumption ratios. The protein amounts given refer to the 700 µl standard assay. Variables are given in bolds. The DT-diaphorase-coupled reactions were run (top section) to completion (no net oxygen consumption) and completeness of NADH oxidation was verified spectrophotometrically at 340 nm using ε_{340} nm = 6.22 mM^{-1} cm^{-1}. The ratios calculated are therefore the quotient of the values given in column 3 and 7 (top section) and in column 5 and 7 (lower two sections). In the remaining samples chemically reduced DPQ was used as a donor. It was quantified spectrophotometrically as given in the methods section. The reactions were run to completion. The data shown represent the mean of at least 3 repetitions (mean ± SE).

PTOX (µg)	Diaph. (µg)	NADH (µM)	DPQ (µM)	$DPQH_2$ (µM)	Act. [nmol O_2 min^{-1} ml^{-1}]	O_2 reduced (µM)	NADH/O_2 $DPQH_2$/O_2
10	10	**25**	100	–	39.2 ± 2.6	13.0 ± 0.5	1.92
10	10	**50**	100	–	78.2 ± 5.3	24.0 ± 1.2	2.08
10	10	**100**	100	–	112.6 ± 6.3	50.0 ± 2.3	2.00
10	10	**200**	100	–	119.4 ± 4.4	105.1 ± 2.1	1.90
10	10	**400**	100	–	129.5 ± 10.2	193.2 ± 3.5	2.07
5	–	–	–	100	52.7 ± 2.4	48.4 ± 1.2	2.07
10	–	–	–	100	116.5 ± 8.4	46.3 ± 1.8	2.15
15	–	–	–	100	177.2 ± 5.7	45.4 ± 2.6	2.20
20	–	–	–	100	229.5 ± 8.3	51.4 ± 2.3	1.94
30	–	–	–	100	228.85 ± 7.9	45.4 ± 1.9	2.20
40	–	–	–	100	237.45 ± 3.7	50.5 ± 1.1	1.98
60	–	–	–	100	239.55 ± 5.6	43.3 ± 1.6	2.30
100	–	–	–	100	243.35 ± 9.8	44.3 ± 1.5	2.25
10	–	–	–	**5.0**	17.2 ± 3.2	3.0 ± 0.2	1.67
10	–	–	–	**12.6**	32.5 ± 4.3	6.0 ± 0.3	2.10
10	–	–	–	**25.0**	51.1 ± 1.6	11.0 ± 0.3	2.30
10	–	–	–	**50.0**	97.8 ± 10.3	26.0 ± 0.5	1.92
10	–	–	–	**100.1**	113.6 ± 7.8	46.0 ± 1.2	2.17
10	–	–	–	**150.2**	123.6 ± 7.1	67.1 ± 3.5	2.24

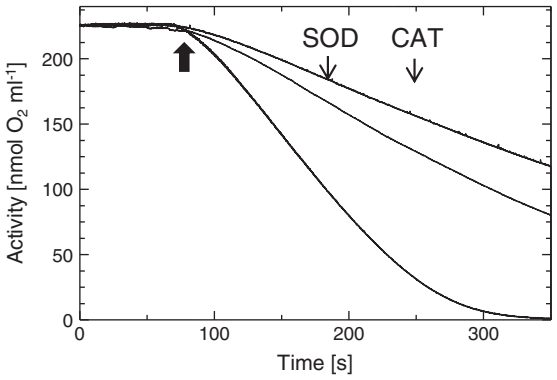

Fig. 6. ROS detection by SOD and CAT. Shown is a octyl-gallate (1 μM) inhibited reaction curve (top); a 1,10-phenantroline (200 μM)-inhibited reaction curve (middle) and a standard reaction curve (bottom). 400 μM NADH were used in the assays to extend the linearity time of reactions. 10 μg of MBP-OsPTOX was pretreated with octyl-gallate or 1,10-phenanthroline at RT for 10 min. The arrowhead indicates the reaction start upon addition of 10 μg DT diaphorase. SOD and CAT were added sequentially, as indicated. The function of SOD and CAT was confirmed by a xanthine oxidase mediated cytochrome c reduction assay and by adding H_2O_2 solution to the oxygen electrode, respectively.

E. coli (cyt *bd*-I, cyt *bd*-II and cyt *bo*) which are not known to be affected by octyl-gallate.

Possible ROS formation was also investigated by EPR using coupled assays with DT-diaphorase in the presence of the hydroxyl radical-specific spin trap 4-POBN (α-(4-pyridyl-1-oxide)-N-tert-butylnitrone), the formation of this ROS species being ensured through Fe-EDTA-mediated Fenton chemistry. With this spin trapping assay we cannot distinguish whether $O_2^{\bullet -}$ or H_2O_2 was originally generated. Two molecules of $O_2^{\bullet -}$ dismutate to H_2O_2 and O_2. In the presence of reduced transition metal ions such as Fe^{2+}, H_2O_2 gives rise to the hydroxyl radical ($HO^{\bullet}$) supported by the reduction of Fe^{3+} by $O_2^{\bullet -}$ (Haber–Weiss reaction). Performing 4-POBN spin trapping in the presence of ethanol is a general procedure to indirectly prove the formation of $HO^{\bullet}$ through the detection of the secondary 4-POBN/α-hydroxyethyl spin adduct.

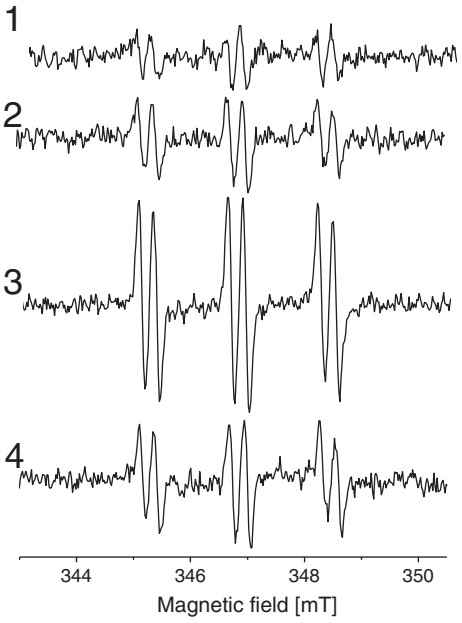

Fig. 7. ROS detection by spin trapping EPR. Shown is the typical 4-POBN/α-hydroxyethyl adduct recorded after 10 min incubation of the samples. Samples contained 38.4 mM DPQ within the lipid phase of liposomes (spectrum 1, 2) or 100 μM DPQ dispersed into the assay from an ethanol stock (spectrum 3, 4), 1 mM NADH, 10 μg of MBP-OsPTOX (spectrum 2, 4), 10 μg DT-diaphorase and the spin trapping assay.

As shown in Fig. 7, a certain amount of reactive oxygen species was generated as a background signal in the presence of NADH, DT diaphorase and DPQ but absence of MBP-OsPTOX (spectra 1 and 3) which may be caused by DT diaphorase activity. The background signal size is about three times larger with freely diffusible $DPQH_2$ (spectrum 3) as compared to liposome-embedded $DPQH_2$ (spectrum 1; the reduced form assuming complete DT diaphorase-mediated reduction). Addition of MBP-OsPTOX increased the signal by about 50% when liposomal $DPQH_2$ was used (compare spectra 1 and 2) while the signal size decreased upon MBP-OsPTOX addition in the case of free $DPQH_2$ (compare spectra 3 and 4). In line with this, catalase, used in parallel assays decreased the O_2 consumption rate with the former and had no effect with the latter samples. This indicates a shift from an antioxidant (water-forming) behavior of MBP-OsPTOX in the case of free $DPQH_2$ to a pro-oxidant (ROS-forming) behavior with the liposomal-bound electron donor.

This pro-oxidant behavior of MBP-Os PTOX at liposomes was investigated in greater detail using pentane-washed liposomes containing different DPQ concentrations within the lipid phase. This revealed at pH 8 that increasing concentrations of the donor led to increased pro-oxidant

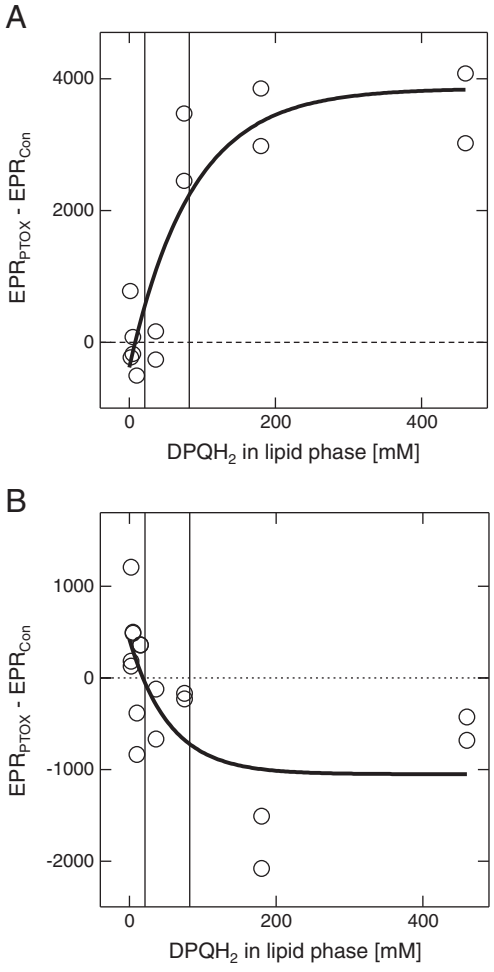

Fig. 8. ROS detection by spin trapping EPR in dependence on the substrate concentration. $EPR_{PTOX} - EPR_{CON}$ refers to the EPR signal size obtained when the background signal with control samples (no PTOX added) was subtracted from the signal size observed with enzymatically active samples (in the presence of PTOX). A: measurements were performed at pH 8.0; B: measurements were performed at pH 6.0. The vertical lines indicate the region of PQ concentrations found in thylakoid membranes. The assays contained the given DPQ concentrations, 200 μM NADH, 10 μg ml^{-1} DT-diaphorase, 10 μg ml^{-1} MBP-OsPTOX, 50 mM 4-POBN, 4% ethanol, and 50 μM FeEDTA. The samples were incubated for 5 min at room temperature prior to measurement.

behavior i.e. increased superoxide and/or H_2O_2 formation (Fig. 8A). Parallel potentiometric measurements and the use of catalase indicated the formation of the latter. At the highest liposomal DPQ(H_2) concentration investigated (460 mM, comp. Fig. 8A), catalase led under standard conditions (200 μM NADH, 10 μg ml^{-1} PTOX, 10 μg ml^{-1} DT diaphorase) to decreased oxygen consumption which fell from 8.4 ± 0.2 μmol O_2 mg^{-1} min^{-1} to 7.7 ± 0.2 μmol O_2 mg^{-1} min^{-1}. This reveals a ROS formation amounting about 1.4 μmol H_2O_2 mg^{-1} min^{-1} equaling about 17% of the total oxygen reducing activity.

Interestingly, the inverse situation was found at more acidic conditions. At pH 6, the system yielded much lower signals and behaved antioxidant, now quenching ROS formation at increasing $DPQH_2$ concentrations while ROS generation was observed at limiting substrate concentration (Fig. 8B). ROS formation could not be measured potentiometrically because catalase is inactive at pH 6. Using the spin trap DEPMPO (5-diethoxyphosphoryl-5-methyl-1-pyrroline *N*-oxide) that forms specific and distinguishable adducts with $O_2^{\bullet-}$ and $HO^{\bullet}$, we aimed to show whether $O_2^{\bullet-}$ or hydrogen peroxide was primarily formed. Using the standard NADH (200 μM) and PTOX (10 μg/ml) concentrations rather small and noisy spectra were obtained (Supplementary Fig. 4). However, the superoxide adduct of DEPMPO can be identified while the lines corresponding to the hydroxyl radical adduct are lacking. Therefore we conclude that it is $O_2^{\bullet-}$ that is generated either by the catalytic center of PTOX itself or by the semiquinone.

Taken together, MBP-OsPTOX is per se very well capable of safely reducing oxygen to water at the expense of $DPQH_2$ without notable formation of oxygen radials. This is the result of our studies carried out in the absence of liposomes, where low $DPQH_2$ concentrations are needed to attain Km. This conflicts with the reports dealing with PTOX-overexpressing plants which bleach under high light conditions [17] and generated $O_2^{\bullet-}$ and $OH^{\bullet}$ [16]. But when membrane bound, much higher $DPQH_2$ concentrations are needed to attain Km and, under these conditions, ROS can form. However, this is pH dependent as well as being dependent on the $DPQH_2$ concentration. A "safety valve" function can be seen at pH 6 at elevated donor concentrations and at pH 8 when donor concentrations are low (Fig. 8).

Plastohydroquinone in photosynthetically active thylakoidal membranes faces a slightly alkaline (about pH 8) stromal environment so that Fig. 8 A mirrors the in vivo situation more closely. Here, the concentrations shown between the vertical lines meet the situation in thylakoids: PQ is extracted from isolated thylakoids at a level of 20–75 mol lipid per mol plastoquinone (1.3–5 mol.%) [38]. The PC concentration within liposomal membranes can be calculated through their partial volume of the biphasic system and the PC amount used (see above) as 1.64 M; consequently the membrane-bound $DPQH_2$ concentration within this partial volume is 21.3–82 mM. At pH 8, this reveals an approximately linear correlation in this concentration range indicating that the photosynthetic activity determining the level of $DPQH_2$ levels lead to increased or decreased ROS formation (at a given protein concentration).Whether the inverse situation at pH 6 is physiologically relevant remains unclear. The 100-fold difference in H^+ impacting $DPQH_2$ acidity (pK of $PQH_2 = 11$; pK of $PQ^{\bullet-} = 7.0$ [39]) may be causal, and can lead to speculate that the PTOX prefers the hydroquinone over the quinone radical, in which case the superoxide observed may result from direct transfer of an electron from $PQ^{\bullet-}$ onto oxygen.

Quinol oxidases (complex III of the respiratory chain and the cyt b_6f complex of the photosynthetic chain) are known to generate superoxide. In these systems the semiquinone serves as reductant for the generation of superoxide. Reduced heme can be an alternative electron donor to oxygen leading to superoxide generation [40]. Analogously, superoxide can be generated by PTOX either through stabilization of the semiquinone or by the reduction of oxygen at the catalytic non-heme diiron center. As shown in Fig. 8, the amount of ROS production is pH-dependent. At pH 8.0, the level of ROS production is higher than at pH 6.0. Furthermore, at pH 8.0 ROS are generated at high quinol concentrations while at pH 6.0 they are generated under substrate limitation. At pH 8.0 the semiquinone is more stable than at pH 6.0 and it appears conceivable that the PTOX-bound stabilized semiquinone acts as a ROS generator. At pH 6.0 the semiquinone is less stable so that oxygen reduction by one electron transfer becomes less favorable. At pH 6.0 under substrate limitation the superoxide may be generated directly at the catalytic center by forming a superoxo-intermediate of the-diiron-center. If, under substrate limitation, the second quinol molecule does not arrive in a timely fashion, the lifetime of this oxygen–iron intermediate may be prolonged turning into a likely source of superoxide.

However, changes in the protein structure can as well be taken into consideration to be involved in the generation of ROS or in the protection against ROS formation. Alternatively, superoxide might be detoxified immediately by a close physical interaction of PTOX with superoxide dismutase. It is known from the non-heme diiron enzyme ribonucleotide reductase that a close interaction between this enzyme and superoxide dismutase is required during the assembly of the active enzyme [41]. Alternatively, a supramolecular organization of PTOX within the photosynthetic electron transfer chain may be considered. In a supercomplex with the cyt b_6f complex, the electron transfer from plastoquinol to PTOX may be well controlled and the probability of superoxide generation be lowered. In this light, the failure in attaining the stoichiometrically correct protein assemblies—as most probably as achieved in PTOX overexpressing plants (see the Introduction)—might well cause the increased ROS production observed. Structural studies are required to approach these questions.

Supplementary data to this article can be found online at http://dx.doi.org/10.1016/j.bbabio.2014.04.007.

Acknowledgments

We are indebted to Mr. Wolfgang Müller, for his help in carrying out the AAS measurements. This work was supported through the European Union Framework Program 7 METAPRO grant 244348.

References

[1] P. Carol, D. Stevenson, C. Bisanz, J. Breitenbach, G. Sandmann, R. Mache, G. Coupland, M. Kuntz, Mutations in the Arabidopsis gene IMMUTANS cause a variegated phenotype by inactivating a chloroplast terminal oxidase associated with phytoene desaturation, Plant Cell 11 (1999) 57–68.
[2] G.P. Rédei, Somatic instability caused by a cysteine-sensitive gene in Arabidopsis, Science 139 (1963) 767–769.
[3] D.A. Berthold, M.E. Andersson, New insight into the structure and function of the alternative oxidase, Biochim. Biophys. Acta 1460 (2000) 241–254.
[4] T. Shiba, Y. Kido, K. Sakamoto, D.K. Inaoka, C. Tsuge, R. Tatsumi, G. Takahashi, E.O. Balogun, T. Nara, T. Aoki, T. Honma, A. Tanaka, M. Inoue, S. Matsuoka, H. Saimoto, A.L. Moore, S. Harada, K. Kita, Structure of the trypanosome cyanide-insensitive alternative oxidase, Proc. Natl. Acad. Sci. U. S. A. 110 (2013) 4580–4585.
[5] T. Joët, B. Genty, E.-M. Josse, M. Kuntz, L. Cournac, G. Peltier, Involvement of a plastid terminal oxidase in plastoquinone oxidation as evidenced by expression of the *Arabidopsis thaliana* enzyme in tobacco, J. Biol. Chem. 277 (2002) 31623–31630.
[6] E.-M. Josse, J.-P. Alcaraz, A.-M. Laboure, M. Kuntz, In vitro characterization of a plastid terminal oxidase (PTOX), Eur. J. Biochem. 270 (2003) 3787–3794.
[7] C.M. Wetzel, C.Z. Jiang, L.J. Meehan, D.F. Voytas, S.R. Rodermel, Nuclear–organelle interactions: the immutans variegation mutant of Arabidopsis is plastid autonomous and impaired in carotenoid biosynthesis, Plant J. 6 (1994) 161–175.
[8] M.P. Mayer, P. Beyer, H. Kleinig, Quinone compounds are able to replace molecular oxygen as terminal electron acceptor in phytoene desaturation in chromoplasts of *Narcissus pseudonarcissus* L, Eur. J. Biochem. 191 (1990) 359–363.
[9] S.R. Norris, T.R. Barrette, D. DellaPenna, Genetic dissection of carotenoid synthesis in Arabidopsis defines plastoquinone as an essential component of phytoene desaturation, Plant Cell 7 (1995) 2139–2149.
[10] V. Nievelstein, J. Vandekerchove, M.H. Tadros, J.V. Lintig, W. Nitschke, P. Beyer, Carotene desaturation is linked to a respiratory redox pathway in *Narcissus pseudonarcissus* chromoplast membranes Involvement of a 23-kDa oxygen-evolving-complex-like protein, Eur. J. Biochem. 233 (1995) 864–872.
[11] M. Shahbazi, M. Gilbert, A.-M. Labouré, M. Kuntz, Dual role of the plastid terminal oxidase in tomato, Plant Physiol. 145 (2007) 691–702.
[12] P. Streb, E.-M. Josse, E. Gallouet, F. Baptist, M. Kuntz, G. Cornic, Evidence for alternative electron sinks to photosynthetic carbon assimilation in the high mountain plant species *Ranunculus glacialis*, Plant Cell Environ. 28 (2005) 1123–1135.
[13] P. Stepien, G.N. Johnson, Contrasting responses of photosynthesis to salt stress in the glycophyte Arabidopsis and the halophyte thellungiella: role of the plastid terminal oxidase as an alternative electron sink, Plant Physiol. 149 (2009) 1154–1165.

[14] M. Díaz, V. De Haro, R. Muñoz, M.J. Quiles, Chlororespiration is involved in the adaptation of Brassica plants to heat and high light intensity, Plant Cell Environ. 30 (2007) 1578–1585.
[15] D. Rosso, A.G. Ivanov, A. Fu, J. Geisler-Lee, L. Hendrickson, M. Geisler, G. Stewart, M. Krol, V. Hurry, S.R. Rodermel, D.P. Maxwell, N.P. Hüner, IMMUTANS does not act as a stress-induced safety valve in the protection of the photosynthetic apparatus of Arabidopsis during steady-state photosynthesis, Plant Physiol. 142 (2006) 574–585.
[16] E. Heyno, C.M. Gross, C. Laureau, M. Culcasi, S. Pietri, A. Krieger-Liszkay, Plastid alternative oxidase (PTOX) promotes oxidative stress when overexpressed in tobacco, J. Biol. Chem. 284 (2009) 31174–31180.
[17] N. Ahmad, F. Michoux, P.J. Nixon, Investigating the production of foreign membrane proteins in tobacco chloroplasts: expression of an algal plastid terminal oxidase, PLoS One 7 (2012) e41722.
[18] M. Trouillard, M. Shahbazi, L. Moyet, F. Rappaport, P. Joliot, M. Kuntz, G. Finazzi, Kinetic properties and physiological role of the plastoquinone terminal oxidase (PTOX) in a vascular plant, Biochim. Biophys. Acta 1817 (2012) 2140–2148.
[19] P. Carol, M. Kuntz, A plastid terminal oxidase comes to light: implications for carotenoid biosynthesis and chlororespiration, Trends Plant Sci. 6 (2001) 31–36.
[20] D. Rumeau, G. Peltier, L. Cournac, Chlororespiration and cyclic electron flow around PSI during photosynthesis and plant stress response, Plant Cell Environ. 30 (2007) 1041–1051.
[21] D. Busso, B. Delagoutte-Busso, D. Moras, Construction of a set Gateway-based destination vectors for high-throughput cloning and expression screening in *Escherichia coli*, Anal. Biochem. 343 (2005) 313–321.
[22] Q. Yu, P. Beyer, Reaction specificities of the ε-ionone-forming lycopene cyclase from rice (*Oryza sativa*) elucidated in vitro, FEBS Lett. 586 (2012) 3415–3420.
[23] Q. Yu, P. Schaub, S. Ghisla, S. Al-Babili, A. Krieger-Liszkay, P. Beyer, The lycopene cyclase CrtY from *Pantoea ananatis* (formerly *Erwinia uredovora*) catalyzes an FADred-dependent non-redox reaction, J. Biol. Chem. 285 (2010) 12109–12120.
[24] Q. Yu, S. Ghisla, J. Hirschberg, V. Mann, P. Beyer, Plant carotene cis-trans isomerase CRTISO: a new member of the FADred-dependent flavoproteins catalyzing non-redox reactions, J. Biol. Chem. 286 (2011) 8666–8676.
[25] P. Schaub, Q. Yu, S. Gemmecker, P. Poussin-Courmontagne, J. Mailliot, A.G. McEwen, S. Ghisla, S. Al-Babili, J. Cavarelli, P. Beyer, On the structure and function of the phytoene desaturase CRTI from *Pantoea ananatis*, a membrane-peripheral and FAD-dependent oxidase/isomerase, PLoS One 7 (2012) e39550.
[26] M. Degli Esposti, E. Bertoli, G. Parenti-Castelli, R. Fato, S. Mascarello, G. Lenaz, Incorporation of ubiquinone homologs into lipid vesicles and mitochondrial membranes, Arch. Biochem. Biophys. 210 (1981) 21–32.
[27] J. Kruk, K. Strzalka, Redox changes of cytochrome b(559) in the presence of plastoquinones, J. Biol. Chem. 276 (2001) 86–91.
[28] A. Dürkop, O.S. Wolfbeis, Nonenzymatic direct assay of hydrogen peroxide at neutral pH using the Eu3Tc fluorescent probe, J. Fluoresc. 15 (2005) 755–761.
[29] M.A.-K. Ragheb, F. Atmeh, Islam M. Arafa, Albumin aggregates: hydrodynamic shape and physico-chemical properties, Jordan J. Chem. 2 (2007) 169–182.
[30] X. Duan, J.A. Hall, H. Nikaido, F.A. Quiocho, Crystal structures of the maltodextrin/maltose-binding protein complexed with reduced oligosaccharides: flexibility of tertiary structure and ligand binding, J. Mol. Biol. 306 (2001) 1115–1126.
[31] D.R. Smyth, M.K. Mrozkiewicz, W.J. Mcgrath, P. Listwan, B. Kobe, Crystal structures of fusion proteins with large-affinity tags, Protein Sci. 12 (2003) 1313–1322.
[32] A.F. Moon, G.A. Mueller, X. Zhong, L.C. Pedersen, A synergistic approach to protein crystallization: combination of a fixed-arm carrier with surface entropy reduction, Protein Sci. 19 (2010) 901–913.
[33] A.I. Greenwood, S. Tristram-Nagle, J.F. Nagle, Partial molecular volumes of lipids and cholesterol, Chem. Phys. Lipids 143 (2006) 1–10.
[34] S. Chen, K. Wu, D. Zhang, M. Sherman, R. Knox, C.S. Yang, Molecular characterization of binding of substrates and inhibitors to DT-diaphorase: combined approach involving site-directed mutagenesis, inhibitor-binding analysis, and computer modeling, Mol. Pharmacol. 56 (1999) 272–278.
[35] D.C. Harris, Determination of iron with 1,10-phenanthroline, Quantitative Chemical Analysis, 6th ed., W.H. Freeman and Comany, New York, 2003, pp. 258–261, (407-422, 453, 461-476, 707-709).
[36] A.L. Moore, T. Shiba, L. Young, S. Harada, K. Kita, K. Ito, Unraveling the heater: new insights into the structure of the alternative oxidase, Annu. Rev. Plant Biol. 64 (2013) 637–663.
[37] R. Bhate, T. Ramasarma, Reinstate hydrogen peroxide as the product of alternative oxidase of plant mitochondria, Indian J. Biochem. Biophys. 47 (2010) 306–310.
[38] M. Blackwell, C. Gibas, S. Gygax, D. Roman, B. Wagner, The plastoquinone diffusion coefficient in chloroplasts and its mechanistic implications, 1183 (1994) 533–543.
[39] B. Ivanov, M. Mubarakshina, S. Khorobrykh, Kinetics of the plastoquinone pool oxidation following illumination. Oxygen incorporation into photosynthetic electron transport chain, FEBS Lett. 581 (2007) 1342–1346.
[40] D. Baniulis, S.S. Hasan, J.T. Stofleth, W.A. Cramer, Mechanism of enhanced superoxide production in the cytochrome b(6)f complex of oxygenic photosynthesis, Biochemistry 52 (2013) 8975–8983.
[41] M. Fontecave, A. Gräslund, P. Reichard, The function of superoxide dismutase during the enzymatic formation of the free radical of ribonucleotide reductase, J. Biol. Chem. 262 (1987) 12332–12346.